crystals

MDPI

Article

Simulation Research on Blood Detection Sensing with Parity-Time Symmetry Structure

Lingjun Yi and Changhong Li *

School of Electronic Information, Qingdao University, Qingdao 266071, China; photoniccrystal@163.com
* Correspondence: jiluch@126.com

Abstract: To realize the design of a medical sensor with excellent comprehensive performance indexes, herein, a plasma concentration sensing model satisfying the Parity-Time (PT) symmetric condition is proposed. In this paper, the transfer matrix method was used to simulate the transmittance spectrum of the structure, according to the amplification effect on defect mode transmission and various detection performance indexes of the structure. We numerically optimized the parameters of the structure, such as the number of PT-symmetry unit cell N, the sample layer thickness d_D as well as the macroscopic Lorentz oscillation intensity α in the PT-symmetry unit cell. The calculation results demonstrate that when the sample concentration changes from 0 g/L to 50 g/L, the wavelength of defect peak shifts from 1538 nm to 1561 nm, and the average quality factor, sensitivity, average figure of merit, average detection limit and average resolution of the structure can reach 78,564, 0.4409 nm/(g/L) (or 227.05 nm/RIU), 11,515 RIU^{-1}, 5.1×10^{-6} RIU and 0.038 g/L, respectively. Not only the sensitivity and resolution of the PT-symmetry structure are better than that of the similar sensors, but it also has excellent comprehensive detection performance, which indicates that the developed sensor can be used in high-precision biomedical detection devices.

Keywords: photonic crystal sensors; parity-time symmetry; transfer matrix method; amplification effect

Citation: Yi, L.; Li, C. Simulation Research on Blood Detection Sensing with Parity-Time Symmetry Structure. *Crystals* **2021**, *11*, 1030. https://doi.org/10.3390/cryst11091030

Academic Editor: Alessandra Toncelli

Received: 6 August 2021
Accepted: 25 August 2021
Published: 27 August 2021

1. Introduction

Compared with traditional sensors, optical sensors can accurately detect signal changes in a variety of complex environments due to the tiny size, high accuracy and strong anti-interference ability, which can be extensively used in many fields such as medicine, national defense, industrial as well as agricultural production [1–7]. In recent years, researchers have introduced sensitive medium layers into the structure or placed the detection sample as a medium layer in the photonic crystal structure. Different types of photonic crystal sensors have been designed based on the theory of photonic crystal [8–12].

One-dimensional photonic crystal (1D-PC) sensors, compared with 2D-PC and 3D-PC sensors, have ultracompact structure, low cost and are sensitive to the change in the refractive index of the defect layer, which has exceptional advantages to achieve the rapid response of the transmittance and reflectance spectrum. Different kinds of high-performance sensor devices were designed utilizing a 1D-PC sensing mechanism. Arafah et al. proposed [13] a novel bio-sensing 1D-PC with analytes as the defect layer, obtaining detection methods for different types of cancer cells based on the changes in transmittance and reflectance spectra with the refractive index of analytes. Ramanujam et al. placed the nanocomposite layer on one side of the cavity layer; the detection sensitivity of 42 nm/RIU~43 nm/RIU was performed by comparing the transmittance peak of cancer cells with that of normal cells [14]. Recently, Jiong et al. realized the detection of the number of Escherichia coli according to the volume fraction of Escherichia coli in different analytes by detecting the offset of the resonance wavelength of 1D-PC [15]. However, the above type of sensing structure has no amplification effect

on the working light wave. Therefore, the transmittance of the defect mode in the photonic forbidden band generally exhibits less than 1. The small transmittance has been demonstrated to greatly affect the practical detection accuracy and reliability of such structures and put forward strict requirements for the spectral detection device. Additionally, the research on the existing medical sensors only considers the sensitivity of the structure or the quality factor and other unilateral performance indicators in most cases, and does not consider the comprehensive performance of the whole structure, which highly affects the actual detection.

Analogue to the Parity-Time (PT) symmetry theory in quantum mechanics, when the refractive index of the gain-loss dielectric layer in the optical structure satisfies the even symmetry of the real part and the odd symmetry of the imaginary part, the structure will satisfy the PT-symmetry condition [16]. Under this condition, novel optical transmission modes will be produced [17–19].

Inspired by this, in view of the performance deficiencies of the above biomedical sensing structures, a PT-symmetry concentration detection structure was designed, which takes a blood sample microcavity as a detection layer. The high-sensitivity and high-resolution blood detection sensing model was obtained by fine PT-symmetry microcavity design and detailed parameter analysis and optimization. Its performance indicators are superior to similar sensors [13,14,20]. Moreover, due to the defect mode amplification effect produced by the PT-symmetry structure, our sensor model has excellent comprehensive detection performance. Based on the sensor model, a medical sensor with high sensitivity and excellent performance can be designed and manufactured. Furthermore, according to its sensing mechanism, it can provide a wider range of applications.

2. Model Design and Theoretical Calculation

Figure 1a shows the proposed PT symmetry microcavity structure that can be expressed as $(ACB)^N D(BCA)^N$. Where A and B identify the loss and gain medium layer, respectively, C represents the matching medium layer, D represents the plasma blood sample layer and N represents the unit cell number of the unilateral Bragg reflectance structure. When the thickness of the A and B layers is equal and the effective refractive index agree with the even symmetry of the real part and the odd symmetry of the imaginary part, the whole structure satisfies the PT-symmetry condition. Under the external pump, the doped quantum dots in the gain medium layer absorb energy by energy level transition. When the structure thoroughly meets the coupling resonance conditions at a specific frequency point, the pump energy will convert into electromagnetic energy of the transmitted light, realizing the amplification of the transmittance.

In the actual blood plasma concentration detection, the optical signal generated by the laser is vertically incident from one end of the structure (as shown in Figure 1b) and the output optical signal at the other end of the structure can be detected by a spectral analyzer. Based on the wavelength information of the output signal, we can realize the detection of blood plasma concentration.

The loss dielectric layer (A layer) and gain dielectric layer (B layer) can be constructed by doping quantum dots in common substrate materials. The refractive index of A and B layers can be quantitatively described by the Lorentz model [21]:

$$n_{(A,B)} = \left(\varepsilon_0 + \frac{\alpha \omega_0^2}{\omega_0^2 - \omega^2 - \omega \gamma i} \right)^{\frac{1}{2}} \quad (1)$$

where ε_0 (= 1.5) is the dielectric constant of the substrate, γ (= 2.5×10^{14} s^{-1}) is the damping coefficient, ω_0 (= 1.216×10^{15} s^{-1}) is the resonant angular frequency, which correspond to the center wavelength of λ_0 (= 1550 nm), ω is the incident light wave angle frequency and α is the macroscopic Lorentz oscillation intensity. It reflects the relationship between system gain, doped quantum dot concentration and excited quantum dot distribution [22]. To make the structure satisfy the PT-symmetry condition, the absolute value of the macroscopic

Lorentz oscillation intensity α in the A layer is required to be equal to that in the B layer; the α symbol represents the gain and the loss. Its value affects the performance of the sensor, as discussed in Section 3.2.

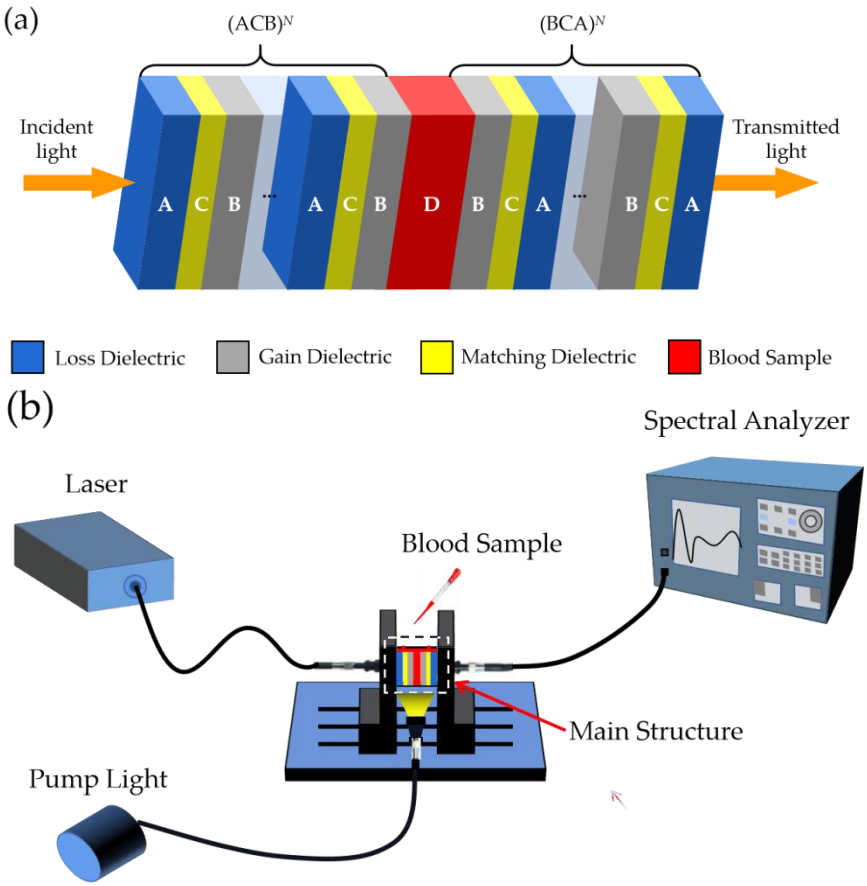

Figure 1. Structure model of PT-symmetry blood sensor. (**a**) Structure model of PT-symmetric blood sensor; (**b**) Schematic diagram of blood detection.

For the sample layer D, when the blood plasma components in the sample change, the blood plasma concentration will also change accordingly, which will then lead to the refractive index of the sample layer to change. The corresponding relationship between the sample refractive index and the blood plasma concentration is calculated with the following formula [20]:

$$n_{\mathrm{D}} = 1.32459 + 0.001942C_{\mathrm{p}} \tag{2}$$

where C_{p} represents blood plasma concentration in blood with unit of g/L. When it comes to the practical measurement, its range is from 0 g/L to 50 g/L. In this calculation, the plasma concentration C_{p} studied varies from 0 g/L to 50 g/L in steps of 10 g/L, and the corresponding refractive index n_{D} ranges from 1.32459 to 1.42169.

Based on the system of Maxwell equations, the relationship between adjacent space fields can be calculated by the transfer matrix method (TMM). If selecting the normal incidence of TE wave as the working light, the transfer matrix of the ith monolayer can be defined by the following matrix [23]:

$$\boldsymbol{M}_i = \begin{bmatrix} \cos\delta_i & -\frac{\mathrm{j}}{\eta_i}\sin\delta_i \\ -\mathrm{j}\eta_i\sin\delta_i & \cos\delta_i \end{bmatrix} \tag{3}$$

where $\eta_i = \sqrt{\frac{\varepsilon_0}{\mu_0}} \cdot n_i$ is the impedance of the ith dielectric layer, $\delta_i = -\frac{\omega}{c} \cdot n_i \cdot d_i$ is the phase shift, d_i represents the thickness of the ith dielectric layer, $\mathrm{j} = \sqrt{-1}$ is the imaginary unit,

ε_0 and μ_0 represent the vacuum dielectric constant and vacuum magnetic conductivity, respectively, and c and ω represent the speed of light in vacuum and incident light angle frequency, respectively. For the designed microcavity structure with $2N + 1$ layer medium, it can be regarded as a cascade of $2N + 1$ transmittance matrices. When light is transmitted in the layered structure, its transmittance equation $\boldsymbol{M}_{\mathrm{PT}}$ and transmittance coefficient t_{PT}, as well as transmittance T_{PT} can be expressed by the following formulas:

$$\boldsymbol{M}_{\mathrm{PT}} = (\boldsymbol{M}_{\mathrm{A}}\boldsymbol{M}_{\mathrm{C}}\boldsymbol{M}_{\mathrm{B}})^{N}\boldsymbol{M}_{\mathrm{D}}(\boldsymbol{M}_{\mathrm{B}}\boldsymbol{M}_{\mathrm{C}}\boldsymbol{M}_{\mathrm{A}})^{N} = \prod_{i=1}^{2N+1}\boldsymbol{M}_i = \begin{bmatrix} m_{11} & m_{12} \\ m_{21} & m_{22} \end{bmatrix} \tag{4}$$

$$t_{\mathrm{PT}} = \frac{2\eta_0}{(m_{11} + m_{12}\eta_1)\eta_0 + (m_{21} + m_{22}\eta_1)} \tag{5}$$

$$T_{\mathrm{PT}} = t_{\mathrm{PT}} \times t_{\mathrm{PT}}^{*} \tag{6}$$

in which η_0 and η_1 represent the impedance of the incident medium and the exit medium, respectively. For the structure designed in this paper, the incident medium and the exit medium are both air.

3. Results and Discussion

In the case of the structural model described in Section 2, initially, the TE wave is selected as the incident light wave in calculation, and the macroscopic Lorentz oscillation intensity is set as $\alpha = 2.3 \times 10^{-4}$. The ZnO_2 dielectric is selected and used as the matching layer C, its refractive index is $n_{\mathrm{C}} = 2$; the number of structural unit cells is $N = 5$. Other structural parameters are the same as given in Section 2. In order to effectively utilize the amplification effect of the structure, the photonic forbidden band is symmetrically distributed about the central wavelength $\lambda_0 = 1550$ nm and the initial thickness of each dielectric layer is adjusted as $d_{\mathrm{A}} = d_{\mathrm{B}} = 1108$ nm, $d_{\mathrm{C}} = 967.3$ nm and $d_{\mathrm{D}} = 2d_{\mathrm{C}}$, respectively.

Based on the above parameters, Figure 2 plots the corresponding transmittance spectrum of the structure when the blood plasma concentration changes from 0 g/L to 50 g/L in steps of 10 g/L. It can be seen from Figure 2 that there is a complete forbidden band in the wavelength range of 1500–1600 nm. The increasing blood plasma concentration causes the whole forbidden band to slightly shift to regions of longer waves while the forbidden band width basically remained unchanged. Consequently, the central position of the forbidden band is still close to the central wavelength $\lambda_0 = 1550$ nm. For the whole PT-symmetry structure, the plasma blood sample layer is equivalent to the defect cavity of the structure, so that the corresponding defect mode (transmittance peak) will come into being in the transmittance band gap of the structure. Surprisingly, we have noticed in this figure that, different from the defect mode of the general photonic crystal structure, the transmittance of the defect mode in the forbidden band is greater than 1. Meanwhile, when the blood plasma concentration changes from 0 g/L to 50 g/L, the position of the transmittance peak in the forbidden band changes from 1529 nm to 1550 nm, and the amplification effect of the structure on the working light wave is gradually increases with the red shift of the transmittance peak. This is predominantly dependent on the strong coupling resonance effect between the PT-symmetry unit and the microcavity, the structure converts pumped energy from the outside into electromagnetic energy of incident light, and thus, the transmittance of defect mode is amplified. In combination with Equation (1), when the working light wavelength is equal to the central wavelength, the refractive index of AB layer accords strictly with the PT-symmetry condition, and the coupling resonance effect of the structure is the strongest. Therefore, the amplification effect of the structure on the working light wave is most obvious at the center wavelength of the forbidden band.

For improving the amplification effect of the structure on the working light wave and enhancing its detection performance in the whole blood plasma concentration range, it is essential to accurately optimize and calibrate the geometric parameters of the structure and material properties of the PT-symmetry dielectric layer. The following analysis focuses on the optimization process of parameters such as unit cell number N of the PT-symmetry

structure and the thickness of the plasma blood sample layer d_D, as well as the influence of macroscopic Lorentz oscillation intensity α in the PT-symmetry dielectric layer on the detection performance.

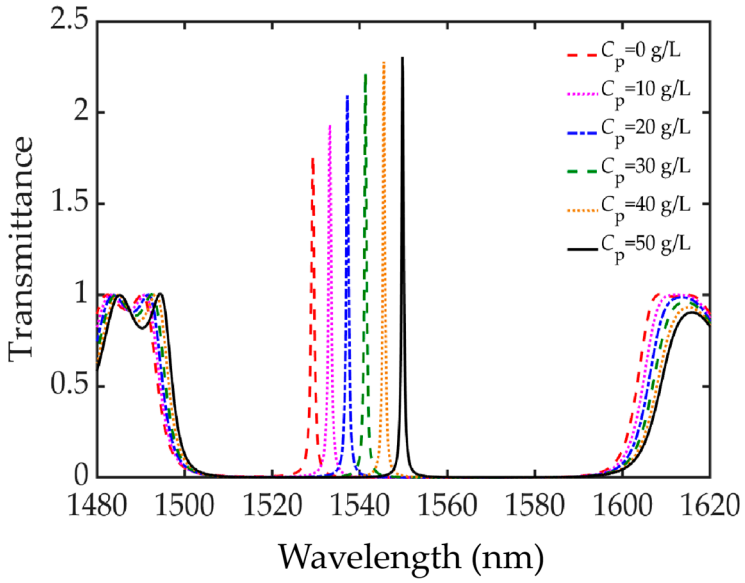

Figure 2. Transmittance spectra of $(ACB)^N D(BCA)^N$ at different blood plasma concentrations.

3.1. Optimization of Unit Cell Number N of PT-Symmetry Structure and Sample Layer Thickness d_D

According to the above analysis, the amplification effect of the structure on the incident light is caused by the PT-symmetry unit. Hence, we need to investigate the influence of the unit cell number N on the amplification effect of the defect mode. Initially, maintaining the other structural parameters as fixed, in Figure 3, the transmittance spectrum at blood plasma concentration of 50 g/L for the structure $(ACB)^N D(BCA)^N$ is shown with the four unit cell values given: N = 5, 6, 7 and 8. Since the unit cell number N has a significant difference in the influence on the transmittance, here, logarithmic transformation, with dB as the unit, is taken for the transmittance during calculation. The transformation relation can be written as: T(dB) = 10lg$T$.

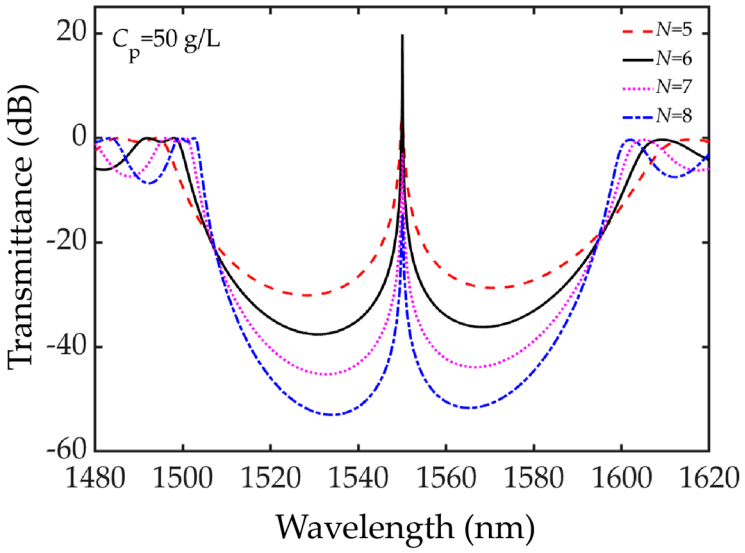

Figure 3. Calculated transmittance spectrum with different unit cell number N.

As shown in Figure 3, when the blood plasma concentration remains unchanged, the inhibition of the structure on the incident light in the forbidden band will gradually fortify

with the increase in N, while the transmittance of the defect mode nonmonotonous change. When N = 5, 6, 7 and 8, the transmittance is 3.532 dB, 19.86 dB, −2.962 dB and −14.69 dB, respectively. It can be seen that the transmittance of the defect mode is largest when N = 6. This indicates that the structure has the strongest amplification effect on the transmittance of defect mode in the center of the forbidden gap. In order to further study the influence of unit cell number N of PT-symmetry structure on the transmittance of defect mode in the whole blood plasma concentration range, we calculated the transmittance of defect mode of the structure $(ACB)^N D(BCA)^N$ in different unit cells with the blood plasma concentration changing from 0 g/L to 50 g/L (taking 10 g/L as a step). The calculation results are shown in Figure 4.

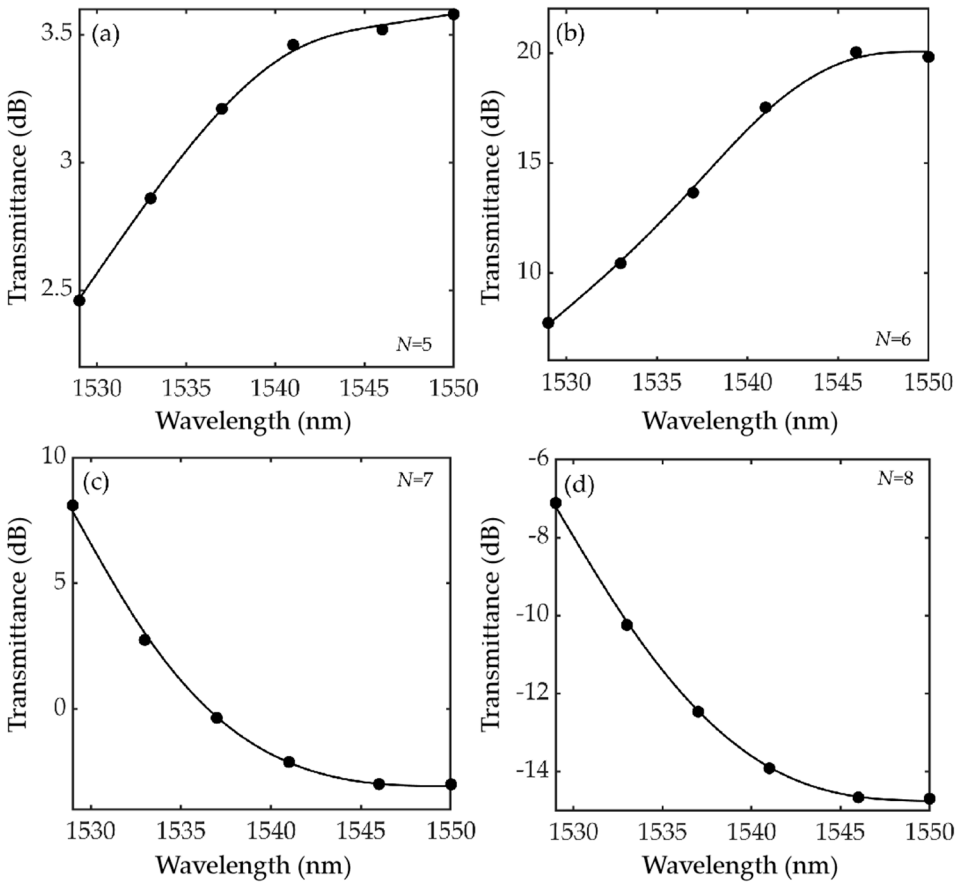

Figure 4. Effect of PT-symmetry unit cell on defect mode transmittance at different blood plasma concentrations. (**a**) N = 5; (**b**) N = 6; (**c**) N = 7; (**d**) N = 8.

As shown in Figure 4, with the increase in blood plasma concentration, the position of defect mode is undergoing an obvious red shift. When N = 5 and 6, the transmittance of defect mode increases with the increase in plasma concentration. On the contrary, when N = 7 and 8, the transmittance of defect mode decreased with the increase in blood plasma concentration. Changing the unit cell number N does not affect the position of defect mode in the case of the same blood plasma concentration, but significantly affects the amplification effect of structure on the transmittance of the defect mode. As the unit cell number N increases from 5 to 8, the transmittance of defect mode firstly increases and then decreases, and reaches the maximum at the same blood plasma concentration when N = 6. This is because the group velocity of the working light wave in the gain layer (B layer) is lower than that in the loss layer (B layer) when N = 6. The photon travels in the gain layer for a relatively longer time, which leaves the energy of the pumped light source more converted into the electromagnetic energy of the working light through the gain layer; accordingly, the structure exhibits an amplification effect. In order to reasonably

take advantage of this amplification effect to improve the detection performance of the structure, we select $N = 6$ as the final optimization result.

In order to ensure the amplification effect of the structure on the transmittance is a suitable match to the whole blood plasma concentration range, so as to avoid affecting the detection performance of the structure due to the small transmittance in the low concentration range, the thickness of the sample layer has been exactly adjusted. When the blood plasma concentration changes from 0 g/L to 50 g/L, the frequency shift range of the transmittance peak can be symmetric with the central wavelength of the forbidden band. Considering that the transmittance peak position is observed in a linear relation with blood plasma concentration. Initially, $C_p = 25$ g/L will be set, the thickness increment Δd_D of the sample layer increases successively from 0 nm with an interval of 10 nm, and the transmittance spectra of structures under different Δd_D are calculated. Figure 5 reveals the variation law of the defect mode position and transmittance along with Δd_D according to the calculation.

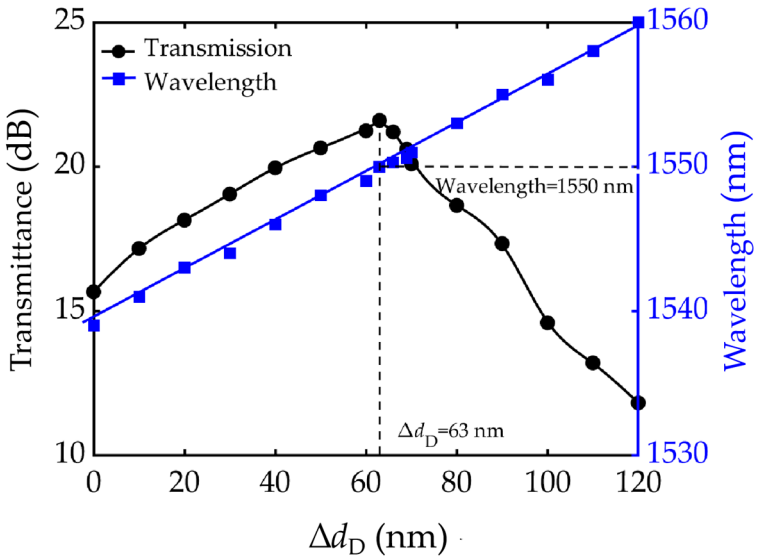

Figure 5. Variation curve of defect mode position and transmittance with the increment of sample layer thickness.

As shown in Figure 5, when Δd_D increased from 0 nm to 63 nm, the position of defect mode moves towards the long-wave direction and the transmittance increases gradually, and the transmittance peak is located at the wavelength of 1550 nm when $\Delta d_D = 63$ nm. Meanwhile, we can readily observe the transmittance of defect mode reaches the maximum when its position is at the strongest coupling point, which corresponds to the position shown by the dotted line in Figure 5. For Δd_D greater than 63 nm, we detect that the transmittance of defect mode decreases accordingly. Therefore, we take the sample increment $\Delta d_D = 63$ nm as the final optimization result and determine the sample layer thickness $d_D = 1999$ nm.

3.2. Detection Mechanism of Blood Plasma Concentration and Analysis of the Structural Performance

Based on the above optimized structural parameters, the transmittance spectrum of the structure at different blood plasma concentration has been calculated. We chose the blood plasma concentration point from 0 g/L to 50 g/L and separated by 10 g/L. The calculation results are shown in Figure 6a. In Figure 6a, we observe the obvious red shift of the transmittance peak motivated by defect mode with the increase in blood plasma concentration. It moves from 1539 nm corresponding, to 0 g/L, and to 1561 nm, corresponding to 50 g/L. Meanwhile, a change in the magnitude of the transmittance peak varies depending on blood plasma concentration. When blood plasma concentration is located in the center of the interval, the PT-symmetry structure results in the signif-

icant amplification of the transmittance of defect mode. When the value of the blood plasma concentration moved from the center of the interval to the high or low concentration interval, the transmittance decreases gradually, and the red shift interval of the whole transmittance peak is distributed symmetrically around the strong coupling point (λ_0 = 1550 nm). In order to facilitate the detection of sample concentration by the position of defect mode, the fitting curve between sample concentration and the position of defect mode is presented in Figure 6. Referring to the calculation results in Figure 6b, the fitting function can be obtained as:

$$\lambda = 0.4409C_p + 1539;\ (R^2 = 0.9999) \quad (7)$$

where C_p and λ are the values of applied blood plasma concentration and transmittance peak position. From Figure 6b, it can be seen that there is a good linear relationship between sample concentration and defect mode position, with a high correlation coefficient up to 0.9999.

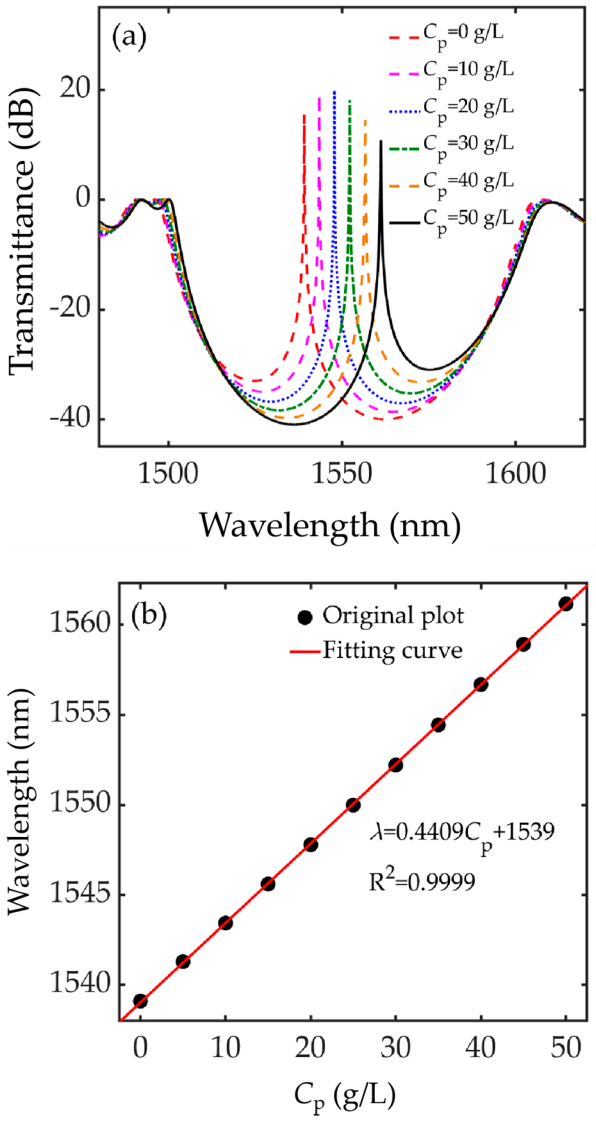

Figure 6. (**a**) Transmittance spectrum and (**b**) linear fitting between defect pattern position and blood plasma concentration of the optimized structure at different blood plasma concentrations.

The sensitivity of the structure can be expressed as the ratio of the wavelength shift amount $\Delta\lambda$ to the sample concentration variation amount ΔC_p or the ratio of the wave-

length shift amount $\Delta\lambda$ to the sample refractive index variation amount Δn, which is defined using the expression [24]:

$$S = \frac{\Delta\lambda}{\Delta \mathrm{Cp}} \text{ or } S = \frac{\Delta\lambda}{\Delta n} \tag{8}$$

Since there is a linear relationship between the sample concentration and shift of the defect mode, the slope of Equation (7)'s fitting line can be regarded as the detection sensitivity of the structure in the whole blood plasma concentration range according to the definition of sensitivity. The calculation result shows that the detection sensitivity of the structure can reach 0.4409 nm/(g/L) (or 227.05 nm/RIU). Therefore, based on the good linear relationship between sample concentration and defect mode position and the high detection sensitivity of the structure, the blood plasma concentration value of the corresponding sample layer can be calculated by detecting the transmittance peak position with Equation (7), so as to realize the detection of the physicochemical properties of plasma blood samples.

In the actual detection, the performance and the efficiency of the sensor is often evaluated by comparing and analyzing multiple indexes, such as the quality factor (Q), the figure of merit (FOM) and detection limit (DL) of the structure. Therefore, according to the calculation results, multiple indexes should be considered to optimize the structural parameters. The quality factor Q is inversely proportional to loss of energy value and directly proportional to stored energy inside the cavity, the greater the Q value is, the more obvious the localization of defect mode is; therefore, a sensor has high Q values that demonstrate that the proposed sensor has very high accuracy because the defect mode has a highly narrow bandwidth [13]. The Q is expressed by the ratio of transmittance peak position λ to the full width at half maximum (FWHM) and can be calculated according to the following equation [25]:

$$\mathrm{Q} = \frac{\lambda}{\mathrm{FWHM}} \tag{9}$$

The ratio between the sensitivity (S) and the FWHM is referred to as the figure of merit (FOM), which is obtained by:

$$\mathrm{FOM} = \frac{S}{\mathrm{FWHM}} = \frac{S \cdot \mathrm{Q}}{\lambda} \tag{10}$$

FOM is proportional to the product of S and Q. The larger the FOM value is, the better the detection performance of the sensor is. The DL is inversely proportional to S and Q, according to [26]:

$$\mathrm{DL} = \frac{\lambda}{20 \cdot S \cdot \mathrm{Q}} \tag{11}$$

The detection limit indicates the smallest detectable refractive index change, it can be seen from Equations (9) and (10) that DL is inversely proportional to FOM. Therefore, the larger the FOM value is, the smaller the detection limit (DL) of the structure is. Meanwhile, combining Equations (9) and (10), (11) can be expressed as:

$$\mathrm{DL} = \frac{\mathrm{FWHM}}{20 \cdot S} \tag{12}$$

When the transmission peak produces a small displacement, the FWHM of the transmission peak can be considered to remain unchanged. Therefore, it can be seen from Equation (12) that DL·S is a fixed value, detection limit (DL) and sensitivity (S) show a trade-off relationship. The smaller the DL of the sensor, the smaller the refractive index change of the detectable blood sample, and the higher the sensitivity S. The simulation results show that adjusting the value of macroscopic Lorentz oscillation intensity α will affect the amplification effect of the structure, change the half-width of the defect mode transmittance peak and then have a great influence on the structure detection performance.

The following section concentrates on the influence of α value on the quality factor, figure of merit and resolution of the structure.

Other structural parameters remain constant, and the blood plasma concentration is set as C_p = 25 g/L to calculate the transmittance of the structure with α value increasing from 2.3×10^{-4} to 2.9×10^{-4} in steps of 0.1×10^{-4}. The 3D plot of the transmittance spectrum is shown in Figure 7, where the position of transmittance peak remains unchanged, while the transmittance shows a tendency to increase first and then decrease with the increscent of α values. When α values range from 2.5×10^{-4} to 2.7×10^{-4}, the amplification effect of structure is most obvious at the same blood plasma concentration. Since adjusting the value of α exclusively changes the gain and loss level of the AB layer and does not affect the position of the transmittance peak in the forbidden band, the value of α does not affect the concentration detection using the fitting result of Equation (7).

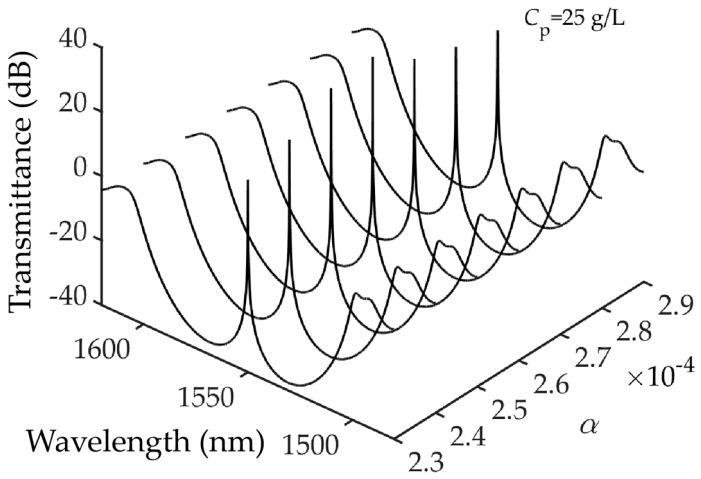

Figure 7. Three-dimensional plot of the transmittance spectra with different values of α.

It can be seen from Equations (9) and (10) that the full width at half maximum FWHM of the transmittance peak affects the quality factor and the figure of merit of the structure, while the FWHM is related to the amplification effect of the structure on the working light, and its value also affects the resolution of the structure. In order to better analyze the influence of α value on the overall detection performance when the blood plasma concentration is detected within the whole range, we calculated the transmittance spectrum at different blood plasma concentrations. When the blood plasma concentrations increase from 0 g/L to 50 g/L, based on Figure 7, we take the average FWHM of the defect mode transmittance peak as a reference factor for analysis. In Figure 8a, we present the variation curve of the average FWHM of the defect mode with α. Considering that the α value is limited by the actual doping process, the α is accurate to 10^{-6} in the calculation.

As can be seen from Figure 8a, the decrease in the average FWHM value of the transmittance peak occurred when α increases from 2.3×10^{-4} to 2.55×10^{-4}, and the minimum value of the average FWHM reaches 0.0238 nm when $\alpha = 2.55 \times 10^{-4}$. As α continues to increase from 2.55×10^{-4} to 2.9×10^{-4}, the average FWHM value increases gradually. In order to further analyze the performance of the structure, we calculate the quality factor and the figure of merit FOM of the structure at different blood plasma concentrations with the same α value, and take the average quality factor and the figure of merit as the detection performance of the structure under the same α value. Figure 8b represents the variation curve of the average quality factor and average figure of merit of the structure with α. It can be seen that when $\alpha = 2.55 \times 10^{-4}$, the average quality factor and the average figure of merit of the structure are the maximum, reaching 78,564 and 11,515 RIU^{-1}, respectively. Therefore, the optimal value of α is 2.55×10^{-4}.

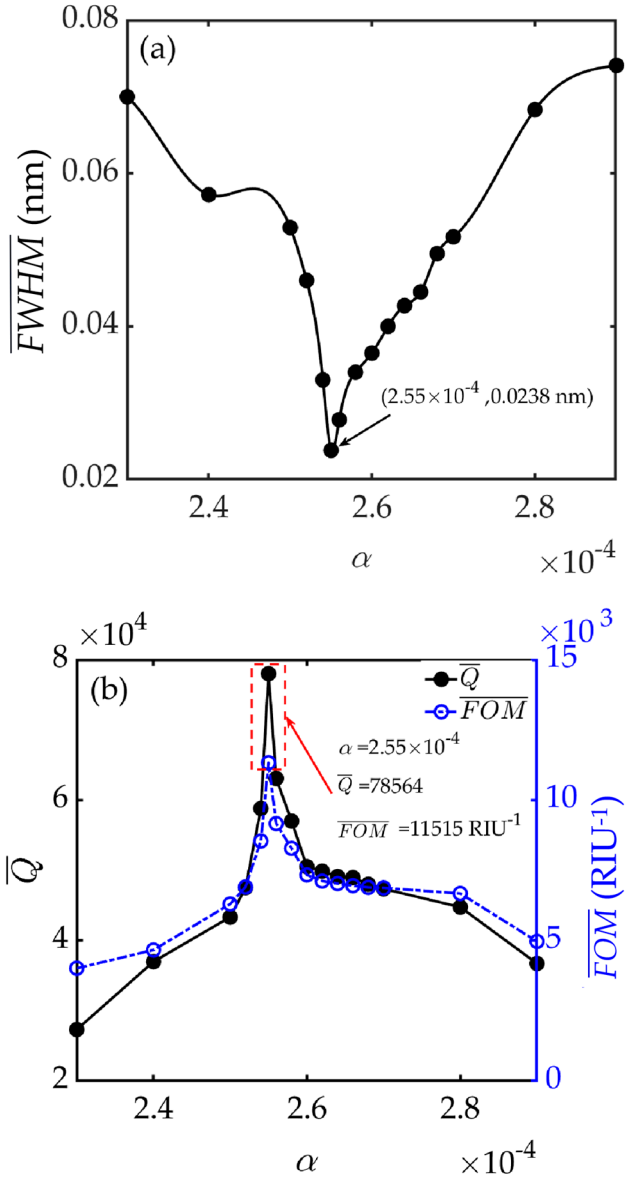

Figure 8. Effect of α on the full width at half maximum of transmittance peak and detection performance. (**a**) The average full width at half maximum varying with α; (**b**) the variation curve of the average quality factor and the average figure of merit varying with α.

For expressing the detection performance parameters of PT-symmetry microcavity structure at $\alpha = 2.55 \times 10^{-4}$ clearly, the data in Figure 8 are extracted. Table 1 shows the full width at half maximum FWHM, quality factor Q and figure of merit FOM at different blood plasma concentrations when $\alpha = 2.55 \times 10^{-4}$; at the same time, Equation (11) is used to calculate the detection limit of the structure at different blood plasma concentrations, the calculation results are listed in Table 1.We have noticed that when the blood plasma concentration is located in the center of the whole interval, the structure shows a compelling detection performance. By contrast, the detection performance decreases in the high and low concentration range. For the whole blood plasma concentration range, the minimum Q, the minimum FOM and the maximum DL of the structure also reaches 22,300, 3244 RIU^{-1} and 12.6 $\times$ 10^{-6} RIU, respectively.

Table 1. The detection performance parameters of PT-symmetry microcavity structure at different blood plasma concentrations ($\alpha = 2.55 \times 10^{-4}$).

C_p/(g/L)	FWHM/nm	Q	FOM/RIU^{-1}	DL/RIU
0	0.03	51,300	7568	5.4×10^{-6}
10	0.025	61,720	9082	4.5×10^{-6}
20	0.01	154,800	22,705	1.8×10^{-6}
30	0.015	103,466	15,137	2.7×10^{-6}
40	0.02	77,800	11,353	3.6×10^{-6}
50	0.07	22,300	3244	12.6×10^{-6}
Average	0.0238	78,564	11,515	5.1×10^{-6}

Resolution is another indicator of the structural performance, which can be described as the minimal detectable blood plasma concentration; the smaller the value, the better the detection performance of the structure. In this paper, the position of the transmittance peak is used for concentration detection, so the resolution can be derived according to the change in blood plasma concentration and the displacement of the transmittance peak. The shift in the defect mode position occurs when the blood plasma concentration changes. For practical detection, the displacement interval of the transmittance peak should be greater than the full width at half maximum of the transmittance peak. As can be seen in the displacement of the transmittance peak of Figure 9a, when C_p = 0 g/L and 0.05 g/L, the interval between the two peaks is 0.0212 nm, which is exactly equal to the full width at half maximum, so the resolution of the structure at 0 g/L is 0.05 g/L. This method can be exploited to measure the structure resolution at different blood plasma concentrations. Since the mean full width at half maximum reaches the minimum value at $\alpha = 2.55 \times 10^{-4}$, and the blood plasma concentration has a good linear relationship with the position of transmittance peak, therefore, the structure had the best resolution in the whole concentration range. According to the relationship between blood plasma concentration and transmittance peak, we plot the resolution of the structure in different blood plasma concentration in Figure 9b. The values are measured based on the thickness of sample layer d_D = 1999 nm, $\alpha = 2.55 \times 10^{-4}$ and N = 6. It can be seen that the resolution of the structure varies from 0.006 g/L to 0.057 g/L in the whole range of blood plasma concentrations. When the blood plasma concentration is between 15 g/L and 25 g/L, the resolution value is relatively small, and the structure detection performance is more remarkable. In the high and low concentration ranges, the resolution is basically maintained at 0.05 g/L, and the average resolution is up to 0.038 g/L for the whole blood plasma concentration range.

Regarding the sensor structure proposed in the literature [20], the maximum detection sensitivity is only 45.06 nm/RIU in the whole blood plasma concentration range, and the full width at half maximum FWHM of the transmittance peak is wider than the frequency shift of the transmittance peak position in the whole blood plasma concentration range, which results in the quality factor, figure of merit and resolution of the structure extremely small. As for the sensor for serum tissue detection proposed in literature [27], although the sensitivity of the structure can reach 6857.89 nm/RIU, the transmittance of the defect mode is lower than 0.4, and the FWHM of the transmittance peak is relatively large, which not only affects the practical application of the structure, but also is not conducive to the signal processing of the detection equipment.

Table 2 shows the optimized structural parameters and the performance of the structure in blood plasma concentration detection. By adjusting and optimizing the plasma blood sample layer d_D =1999 nm, the cycle of PT-symmetry unit N = 6, and the macroscopic Lorentz oscillation intensity $\alpha = 2.55 \times 10^{-4}$, under these conditions, the structure is used to detect the plasma blood samples with blood plasma concentration from 0 g/L to 50 g/L. Its sensitivity, average quality factor, average figure of merit, average detection limit and average resolution are 0.4409 nm/(g/L) (or 227.05 nm/RIU), 78,564, 11,515 RIU^{-1}, 5.1×10^{-6} RIU and 0.038 g/L, respectively. Compared with other research on biomedical sensors, the detection performance of the structure is comprehensively analyzed in this pa-

per, and each performance index is improved synchronously. The reported results indicate that the structure has potential application value in blood detection.

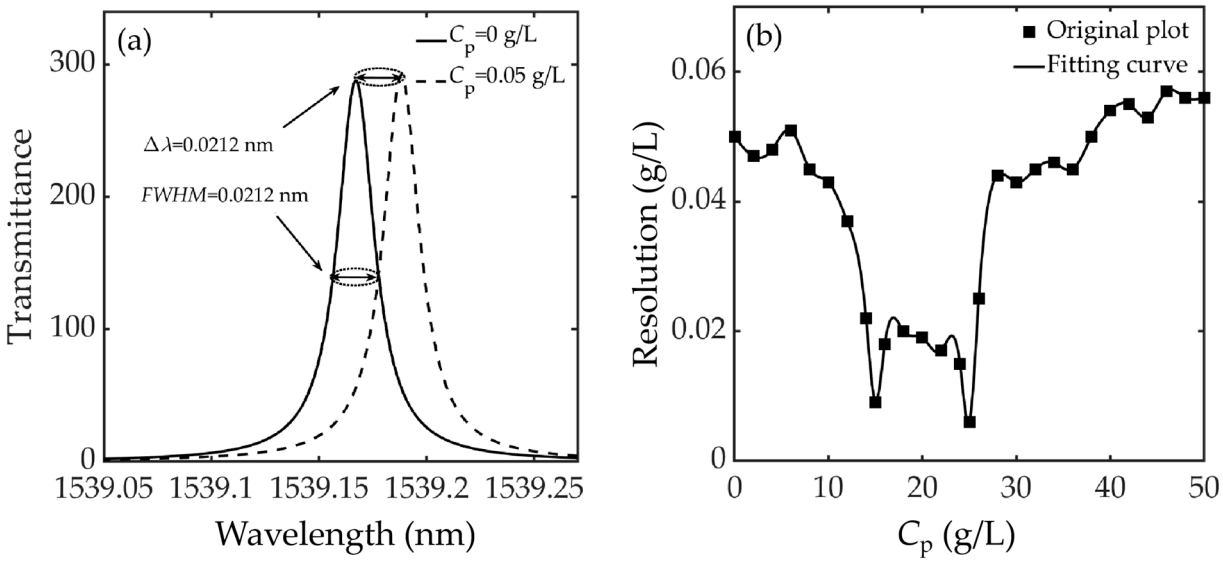

Figure 9. Structure resolution. (**a**) Calculation of structural resolution by peak interval; (**b**) resolution of the structure in detecting different blood plasma concentrations.

Table 2. Optimized parameters and detection performance of the structure $(ACB)^N D(BCA)^N$.

Structure Parameters			Performance Indexes				
Thickness	***N***	***α***	***S***	$\overline{\mathbf{Q}}$	$\overline{\mathbf{FOM}}$	$\overline{\mathbf{DL}}$	**Average Resolution**
$d_A = d_B$ = 1108 nm d_C = 968 nm d_D = 1999 nm	6	2.55×10^{-4}	0.4409 nm/(g/L) or 227.05 nm/RIU	78,564	11,515 RIU^{-1}	5.1×10^{-6} RIU	0.038 g/L

4. Conclusions

On account of the PT-symmetry theory, a novel medical detection model $(ACB)^N D(BCA)^N$ is developed in this paper. The plasma blood sample is embedded in the PT-symmetry layered structure to pattern a resonant microcavity. The blood plasma concentration can be detected against the position of defect mode in the forbidden band. Owing to the PT-symmetry condition, the transmittance of the defect mode is amplified by the structure, which is not only more conducive to the signal collection of detection equipment but can also significantly improve the detection performance of the structure on blood plasma concentration. Through the optimization design of the structure—when the plasma blood sample layer d_D = 1999 nm, the unit cell number N = 6 and the macroscopic Lorentz oscillation intensity $\alpha = 2.55 \times 10^{-4}$—we find that the detection sensitivity of the structure can reach 0.4409 nm/(g/L) (or 227.05 nm/RIU) for the plasma blood samples with concentration from 0 g/L to 50 g/L, and the linear fitting coefficient can reach 0.9999. The average quality factor, average figure of merit, average detection limit and average resolution can reach 78,564, 11,515 RIU^{-1}, 5.1×10^{-6} RIU and 0.038 g/L, respectively. This design has attractive advantages such as a simple structure, better comprehensive performance and small mode volume compared with the traditional 2D photonic crystal fiber sensor and the complex 1D-PC sensor with a special material layer. These characteristics indicate that the research has certain reference significance for the design of high-performance biomedical sensor devices.

Author Contributions: L.Y. and C.L. conceived the idea of the paper; L.Y. designed and performed the simulations and wrote the original draft; L.Y. and C.L. discussed the results and modified the manuscript. All authors have read and agreed to the published version of the manuscript.

Funding: This research was funded by the National Natural Science Foundation of China (NSFC) with grant numbers 61307050 and 61701271 and the Natural Science Foundation of Shandong Province with grant number ZR2016AM27.

Acknowledgments: The authors sincerely acknowledge the financial support of the National Natural Science Foundation of China (Nos. 61307050 and 61701271), as well as the Natural Science Foundation of Shandong Province (No. ZR2016AM27).

Conflicts of Interest: The authors declare no conflict of interest.

References

1. Malmir, N.; Fasihi, K. Highly-Sensitive Label-Free Biosensor Based on Two Dimensional Photonic Crystals with Negative Refraction. *J. Mod. Opt.* **2017**, *64*, 1346828. [CrossRef]
2. Bugay, A.N.; Khalyapin, V.A. Analytic Description of Pulse Frequency Self-shift in Nonlinear Photonic Crystal Fibers. *Commun. Nonlinear* **2019**, *75*, 270–279. [CrossRef]
3. Xiao, G.L.; Zhang, K.F.; Yang, H.Y.; Yang, Y.T.; Yang, X.H.; Dou, W.Y.; Zeng, L.Z. Refractive Index Sensor with Double Resonance Peaks for D-Type Symmetric Two-Core Photonic Crystal Fiber. *Acta Opt. Sin.* **2020**, *40*, 1206001. [CrossRef]
4. Amoudache, S.; Pennec, Y.; Rouhani, B.D.; Khater, A.; Lucklum, R.; Tigrine, R. Simultaneous Sensing of Light and Sound Velocities of Fluids in a Two-Dimensional Photonic Crystal with Defects. *J. Appl. Phys.* **2014**, *115*, 134503. [CrossRef]
5. Amoudache, S.; Moiseyenko, R.; Pennec, Y.; Rouhani, B.D.; Khater, A.; Lucklum, R.; Tigrine, R. Optical and Acoustic Sensing Using Fano-Like Resonances in Dual Phononic and Photonic Crystal Plate. *J. Appl. Phys.* **2016**, *119*, 114502. [CrossRef]
6. Yang, D.-Q.; Chen, J.H.; Cao, Q.T.; Duan, B.; Chen, H.J.; Yu, X.C.; Xiao, Y.F. Operando monitoring transition dynamics of responsive polymer using optofluidic microcavities. *Light Sci. Appl.* **2021**, *10*, 128. [CrossRef] [PubMed]
7. Yang, D.-Q.; Wang, A.Q.; Chen, J.H.; Yu, X.C.; Lan, C.W.; Ji, Y.F.; Xiao, Y.F. Real-time monitoring of hydrogel phase transition in an ultrahigh Q microbubble resonator. *Photon. Res.* **2020**, *8*, 497–502. [CrossRef]
8. Song, Y.; Bai, J.; Zhang, R.; Wu, E.; Wang, J.; Li, S.; Ning, B.; Wang, M.; Gao, Z.; Peng, Y. LSPR-Enhanced Photonic Crystal Allows Ultrasensitive and Label-Free Detection of Hazardous Chemicals. *Sens. Actuators B* **2020**, *310*, 127671. [CrossRef]
9. Jahani, D.; Raissi, B.; Taati, F.; Riahifar, R.; Yaghmaee, M.S. Optical Properties of Fluidic Defect States in One-Dimensional Graphene-Based Photonic Crystal Biosensors: Visible and Infrared Hall Regime Sensing. *Eur. Phys. J. Plus* **2020**, *135*, 160. [CrossRef]
10. Herrera, A.; Calero, J.; Porras, M.N. Pressure, Temperature, and Thickness Dependence of Transmittance in a 1D Superconductor-Semiconductor Photonic Crystal. *J. Appl. Phys.* **2018**, *123*, 033101. [CrossRef]
11. Goyal, A.K.; Dutta, H.S.; Pal, S. Recent Advances and Progress in Photonic Crystal-Based Gas Sensors. *J. Phys. D Appl. Phys.* **2017**, *50*, 203001. [CrossRef]
12. Yang, D.-Q.; Duan, B.; Liu, X.; Wang, A.-Q.; Li, X.-G.; Ji, Y.-F. Photonic Crystal Nanobeam Cavities for Nanoscale Optical Sensing: A review. *Micromachines* **2020**, *11*, 72. [CrossRef]
13. Aly, A.H.; Zaky, Z.A. Ultra-sensitive Photonic Crystal Cancer Cells Sensor with a High-Quality Factor. *Cryogenics* **2019**, *104*, 102991. [CrossRef]
14. Ramanujam, N.R.; Amiri, I.S.; Taya, A.; Olyaee, S.; Udaiyakumar, R.; Pandian, A.P.; Joseph, K.S.; Mahalakshmi, P.; Yupapin, P.P. Enhanced Sensitivity of Cancer Cell Using one Dimensional Nano Composite Material Coated Photonic Crystal. *Microsyst. Technol.* **2019**, *25*, 189–196. [CrossRef]
15. Hao, J.J.; Xie, X.; Gu, K.D.; Du, W.C.; Liu, Y.J.; Yang, H.W. Research on Photonic Crystal–Based Biosensor for Detection of Escherichia coli Colony. *Plasmonics* **2019**, *14*, 1919–1928. [CrossRef]
16. Konotop, V.V.; Yang, J.; Zezyulin, D.A. Nonlinear Waves in PT-Symmetric Systems. *Rev. Mod. Phys.* **2016**, *88*, 035002. [CrossRef]
17. Fang, Y.T.; Zhang, Y.C.; Wang, J.J. Resonance-Dependent Extraordinary Reflection and Transmission in PT-Symmetric layered Structure. *Opt. Commun.* **2018**, *407*, 255–261. [CrossRef]
18. Peng, B.; Özdemir, S.K.; Lei, F. Parity-Time-Symmetric Whispering-Gallery Microcavities. *Nat. Phys.* **2014**, *10*, 394–398. [CrossRef]
19. Maryam, S.; Mohamed, F.; Chen, P.Y. PT-Symmetric Metasurfaces: Wave Manipulation and Sensing Using Singular Points. *New J. Phys.* **2017**, *19*, 065002.
20. El-Khozondar, H.J.; Mahalakshmi, P.; El-Khozondar, R.J.; Ramanujam, N.R.; Amiri, I.S.; Yupapin, P. Design of One Dimensional Refractive Index Sensor Using Ternary Photonic Crystal Waveguide for Plasma Blood Samples Applications. *Phys. Rev. E* **2019**, *111*, 29–36. [CrossRef]
21. Zhang, Y.C.; Jiang, X.M.; Xia, J.; Fang, Y.T. Tunable High Sensitivity Temperature Sensor Based on Transmittance Changes of Parity-Time Symmetry Structure. *Chin. J. Lase.* **2018**, *45*, 0710002. [CrossRef]
22. Govyadinov, A.A.; Podolskiy, V.A.; Noginov, M.A. Active Metamaterials: Sign of Refractive Index and Gain-Assisted Dispersion Management. *Appl. Phys. Lett.* **2007**, *91*, 191103. [CrossRef]
23. Jao, R.-F.; Lin, M.-C. Quantitative Analysis of Photon Density of States for One-Dimensional Photonic Crystals in a Rectangular Waveguide. *Crystals* **2019**, *9*, 576. [CrossRef]
24. Li, T.; Gao, D.; Zhang, D.; Cassan, E. High-Q and High-Sensitivity One-Dimensional Photonic Crystal Slot Nanobeam Cavity Sensors. *IEEE Photon. Technol. Lett.* **2016**, *28*, 689–692. [CrossRef]

25. Cheng, P.-J.; Huang, Z.-T.; Li, J.-H.; Chou, B.-T.; Chou, Y.-H.; Lo, W.-C.; Chen, K.-P.; Lu, T.-C.; Lin, T.-R. High-Performance Plasmonic Nanolasers with a Nanotrench Defect Cavity for Sensing Applications. *ACS Photon.* **2018**, *5*, 2638–2644. [CrossRef]
26. Beheiry, E.; Liu, M.; Fan, V.; Levi, S. Sensitivity enhancement in photonic crystal slab biosensors. *Opt. Express* **2010**, *18*, 22702–22714. [CrossRef] [PubMed]
27. Hao, J.J.; Gu, K.D.; Lei, X.; Liu, Y.J.; Yang, Z.F.; Yang, H.W. Research on Low-Temperature Blood Tissues Detection Biosensor Based on One-Dimensional Superconducting Photonic Crystal. *Commun. Nonlinear* **2020**, *89*, 105299. [CrossRef]